Remote sensing of CO, CH4 , and O3 using a spaceborne nadir-viewing interferometer

Cathy Clerbaux, P. Chazette, Juliette Hadji-Lazaro, Gérard Mégie, J.-F. Müller, S. Clough

JOURNAL OF GEOPHYSICAL RESEARCH, VOL. 103, NO. D15, PAGES 18,999–19,013, AUGUST 20, 1998

Remote sensing of CO, CH_4, and O_3 using a spaceborne nadir-viewing interferometer

C. Clerbaux,[1] P. Chazette,[2] J. Hadji-Lazaro,[1] G. Mégie,[1] J.-F. Müller,[3] and S. A. Clough[4]

Abstract. Within the next 5 years, several instruments launched on polar orbiting satellites will provide high-resolution infrared remote-sensing measurements of CO, CH_4, and O_3 on a global scale. The upwelling spectral radiances to be recorded by a nadir-looking remote sensor have been simulated using a high-resolution radiative code (line-by-line radiative transfer model (LBLRTM)) coupled to a three-dimensional chemical transport model (intermediate model of the annual and global evolution of species (IMAGES)). The instrumental specifications of the Fourier transform interferometric monitor for greenhouse gases/Advanced Earth Observing System (IMG/ADEOS) and infrared atmospheric sounding interferometer (IASI/METOP) were used to generate realistic data. Calculations have been performed to assess the sensitivity of the nadir spectral radiances to changes in the gas concentration, temperature profile and to instrumental characteristics. We provide spectral intervals for an efficient retrieval of these species, together with a set of climatological tropospheric standard mixing ratio profiles.

1. Introduction

Global scale measurements of trace gases are required to understand tropospheric chemistry and to estimate the possible radiative forcing of climate due to increasing concentrations of greenhouse gases [*World Meteorological Organization (WMO)*, 1995; *Intergovernmental Panel on Climate Change (IPCC)*, 1996]. Ozone (O_3) and two of its main precursors, carbon monoxide (CO) and methane (CH_4), are strongly coupled through chemical reactions involving the hydroxyl radical (OH). The photolysis ($\lambda < 310$ nm) of tropospheric O_3 is followed by reaction of the oxygen atom $O(^1D)$ with water vapor (H_2O), producing OH. Reaction with OH provides the dominant loss mechanism of many atmospheric pollutants. The oxidation cycles of both CH_4 and CO either produce or destroy O_3 depending on the level of concentration of nitric oxide [*Crutzen*, 1973; *Logan et al.*, 1981]. As a consequence, a change in the concentration of one of these species modifies the oxidizing capacity of the troposphere and hence affects the lifetimes and abundances of many other trace gases.

At the beginning of the 1990s, important changes in CO and CH_4 growth rates were reported [*Novelli et al.*, 1994; *Dlugokencky et al.*, 1994], and the understanding of these changes in term of sources and sinks has been the focus of several studies [*Dlugokencky et al.*, 1996; *Granier et al.*, 1996]. Despite this effort, large uncertainties remain on the estimated strengths of sources and sinks of the main trace gases [*WMO*, 1995]. These uncertainties could only be resolved from the simultaneously measured distributions of sources gases (CO and CH_4) and O_3 together with chemical transport models (CTMs) using inverse calculation methods [*Brown*, 1995] and data assimilation techniques [*Fisher and Lary*, 1995]. Global budgets for these species would constrain the oxidizing power of the troposphere and thus infer the global distribution of OH, which is not directly measurable from space. The impact of biomass burning could also be analyzed from these observations.

This has heightened interest in developing global scale measurements using ground-based networks [*Novelli et al.*, 1992; *Dlugokencky et al* , 1994] and spaceborne remote sensors. The ground-based measurements, using gas bottle sampling and gas chromatography, provide accurate data but are restricted in spatial coverage. Only a limited picture of the distribution of species like CO and O_3 can be obtained. Remote sensors provide global scale measurements but with an order of magnitude lower accuracy. Several nadir-viewing instru-

[1]Service d'Aéronomie du CNRS, Institut Pierre-Simon Laplace, Paris, France.

[2]Laboratoire des Sciences. du Climat et de l'Environnement CEA, Institut Pierre-Simon Laplace, Saclay, France.

[3]Belgian Institute for Space Aeronomy, Brussels.

[4]Atmospheric and Environmental Research, Inc., Cambridge, Massachusetts.

Paper number 98JD01422.
0148-0227/98/98JD-01422$09.00

ments dedicated to the sounding of the troposphere are planned for launch on polar orbiting satellites within the coming decade. A summary of the ongoing and forthcoming missions is presented in Table 1. The interferometric monitor for greenhouse gases (IMG) instrument was launched aboard the Japanese Advanced Earth Observing System (ADEOS) on August 17, 1996, and stopped operating after 10 months, on June 30, 1997. The measurements of pollution in the troposphere (MOPITT) instrument is scheduled for launch in October 1998 as part of NASA's EOS-AM1 payload. The atmospheric infrared sounder (AIRS) will fly on the EOS-PM1 spacecraft in the years 2000. The infrared atmospheric sounding interferometer (IASI) will be carried by the European Operational Meteorology (METOP) platform, to be launched around 2002. The tropospheric emission spectrometer (TES) will probably be part of the EOS-CHEM1 satellite early in the next century. All these instruments record atmospheric spectra using the thermal emission of Earth as a source. According to their main mission objectives, they use different instrumental device, spectral resolution, and spatial and temporal samplings. AIRS and IASI belong to the next generation of temperature and humidity sounders for operational weather forecasting. MOPITT is designed to measure the global distribution of tropospheric CO and CH_4. IMG and TES are both high resolution interferometers primarily dedicated to chemistry and climate research. Owing to their nadir-viewing recording geometry, these instruments are mostly sensitive to the tropospheric part of the atmosphere, except for TES, which will also be able to scan the stratosphere thanks to its combined limb and nadir-viewing modes.

From data provided by these instruments it will be possible to retrieve information on many geophysical variables. Preliminary studies were undertaken to assess the extent to which concentrations of infrared-absorbing molecules could be retrieved with useful accuracy from upwelling spectral radiances [*Wetzel et al.*, 1995]. In order to prepare these missions, fast forward radiative codes [*Clough et al.*, 1992; *Clough and Iacono*, 1995; *Cheruy et al.*, 1995; *Pan et al.*, 1995] and efficient algorithms for the retrieval of trace gases from measured nadir radiances are under development [*Clough et al.*, 1995; *Clerbaux et al.*, 1995; *McMillan et al.*, 1996].

This paper aims to present the information content and sensitivity studies undertaken in the framework of the development of an inversion algorithm to retrieve CO, CH_4, and O_3 from infrared atmospheric spectra recorded by a nadir-looking Fourier transform interferometer [*Clerbaux et al.*, 1995]. Inversion results are not reported in this paper, which attempts to estimate the uncertainties on radiances provided by IMG and IASI and compare the measurement accuracy to the variability of each molecule. A realistic database of simulated measurements has been created (section 2), and relevant spectral intervals for an efficient retrieval have been selected (section 3). The contribution of geophysical variables (concentration and temperature) and instrumental characteristics (noise and resolution) to the recorded nadir radiances has been analyzed, and the expected variability of each species is estimated from the CTM (section 4). A reduced climatological database with representative profiles for each species is provided (section 5).

2. Simulation of Nadir Radiance Spectra

In order to build a comprehensive database to make sensitivity studies and test inversion algorithms, we have coupled the atmospheric concentration profiles provided by the three-dimensional tropospheric chemical transport model IMAGES (intermediate model of the annual and global evolution of species) [*Müller and Brasseur*, 1995] to the line-by-line radiative code LBLRTM [*Clough et al.*, 1992; *Clough and Iacono*, 1995] and then convolved these spectra with either the IMG or IASI instrumental function. The two models have been extensively validated against observational data, and their main characteristics are briefly reported here, along with the instrumental specifications of IASI and IMG.

2.1. Chemical Transport Model

The intermediate model of the annual and global evolution of species (IMAGES) is a three-dimensional chemical transport model of the troposphere. It extends from the surface to the lower stratosphere (50 hPa) with a horizontal resolution of 5° in latitude and longitude, and includes 25 σ-levels in the vertical. It

Table 1. Nadir-Viewing Remote Sensors Providing Simultaneous Measurements of O_3, CO, and CH_4 in the Infrared, Using the Thermal Emission of Earth as a Source

Instrument	Platform	Device	Launch date	Reference
IMG	ADEOS	Fourier transform interferometer	Aug. 1996	*Ogawa et al.* [1994]
MOPITT[a]	EOS-AM1	gas correlation spectrometer	Oct. 1998	*Drummond and Mand* [1996]
AIRS	EOS-PM1	grating array spectrometer	2000	*Aumann and Miller* [1995]
IASI	METOP	Fourier transform interferometer	2002	*Cayla and Javelle* [1995]
TES	EOS-CHEM1	Fourier transform interferometer	2002	*Beer and Glavich* [1989]

[a] Measures only CO and CH_4.

provides the distribution of 41 chemical compounds, including CO, CH_4, and O_3. The chemical mechanisms include 125 chemical reactions and 26 photodissociation reactions. The model accounts for chemical transformation, surfaces emissions (emissions from biogenic and anthropogenic sources), and dry and wet depositions. The transport of long-lived chemical species is simulated by a semi-Lagrangian advection scheme on the basis of monthly mean climatological winds and temperatures provided by the European Center for Medium Range Weather Forecasts (ECMWF). The effect of wind variability at timescales shorter than a month is formulated through an eddy diffusion parametrization. Convection transport is also parametrized. The distribution of clouds, eddy diffusion coefficients, and the boundary conditions are monthly means constrained by observational data.

2.2. Radiative Transfer Model

The forward model used in this study is the line-by-line radiative transfer model (LBLRTM, version 4.2), which is an improved and accelerated version of FASCODE [*Clough et al.*, 1992; *Clough and Iacono*, 1995]. It has been parametrized for nadir-viewing geometry to simulate the infrared radiation emitted and absorbed by the Earth-atmosphere system along the optical path. High-resolution atmospheric radiances have been generated for cloud and aerosol-free conditions. In this model, the line parameters for radiance calculations are provided by the HITRAN 92 spectroscopic database [*Rothman et al.*, 1992]. The Voigt line shape is used at all atmospheric levels with an algorithm based on a linear combination of approximating functions. An algorithm is implemented for the treatment of the variation of the Planck function within a vertically inhomogeneous layer. LBLRTM incorporates a full water vapor continuum model (CKD_2.2), validated against atmospheric observations. Continua for carbon dioxide, oxygen, and nitrogen are also included.

2.3. Instrumental Function and Radiometric Noise

The high-resolution simulated radiances obtained by introducing the IMAGES mixing ratio profiles of CO, CH_4, and O_3 into LBLRTM were convolved with the IMG and IASI instrumental response functions. The main instrumental characteristics of these two spectrometers are reported in Table 2. They were optimized taking into account the constraints associated with their main mission objectives, which are climate research for IMG and operational meteorology for IASI. This results in a trade-off between spectral resolution and horizontal sampling. The IMG spectrometer records atmospheric spectra using an optical path difference (OPD) of 10 cm, which corresponds to a spectral resolution, defined as the full width at half maximum (FWHM) of the spectral response function, of 0.1 cm^{-1} after a Gaussian apodization. The data are sampled at twice the Nyquist sampling frequency.

Table 2. Instrumental Characteristics for IMG and IASI

	IMG	IASI
Spectral range, cm^{-1}	714-3030	645-2760
Optical path difference, cm	10	2
Number of pixels	1	4
Footprint, km	8	12
Total scan cycle time, s	110	8

IASI has a squared field of view sampled by a matrix of 2×2 circular pixels of 12 km each and will provide measurements with a good horizontal coverage due to its ability to scan across track with a swath width of ±1100 km. Owing to the off-axis position of the detectors in the focal plane, the IASI instrument spectral response function (ISRF) and hence the spectral resolution associated with its OPD of 2 cm are wavenumber dependent. With increasing wavenumbers, the theoretical sinc function is broadened by off-axis effects and becomes asymmetrical. The associated spectral resolution in terms of FWHM is provided as a function of wavenumbers in Figure 1 [*Camy-Peyret and Payan*, 1997].

For technological reasons, the full spectral range covered by these instruments is subdivided in three spectral bands with different radiometric noise associated with the performance of each detector. The instrumental noise (in $mW/(m^2\ cm^{-1}\ sr)$) of each instrument is plotted in Figure 2. For example, Figure 3 represents a high-resolution spectrum in the spectral range used for CO retrieval as well as the simulated radiances for both IMG and IASI instruments, taking into account spectral resolution, sampling, and radiometric noise.

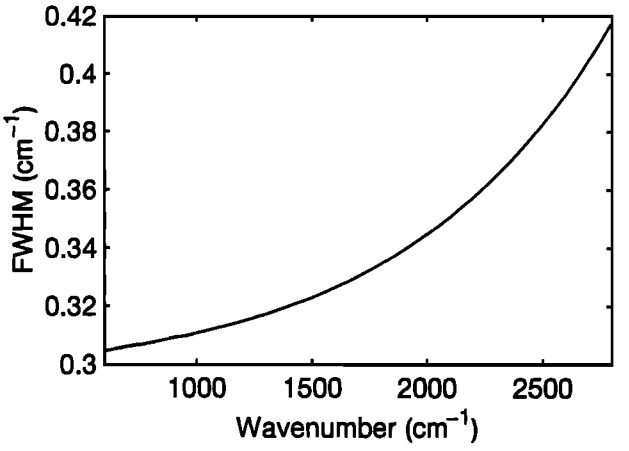

Figure 1. Spectral resolution (full with at half maximum) as a function of wavenumber, calculated using the IASI instrumental function (unapodized).

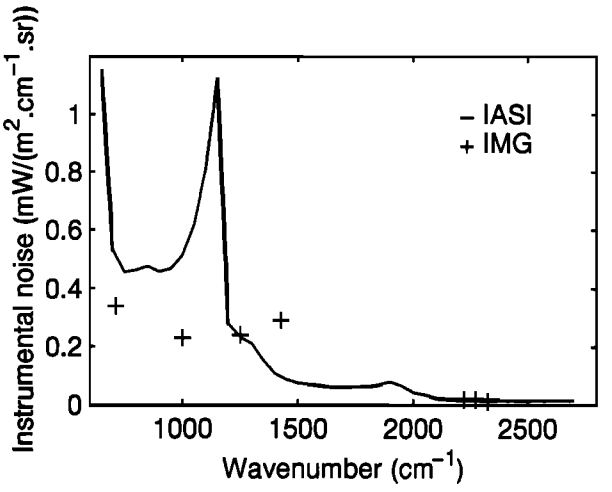

Figure 2. Radiometric instrumental noise for IASI and IMG.

3. Spectral Interval Selection

The spectral signature of atmospheric molecules which absorb in the infrared spectral range and present high concentration levels may be analyzed from the spectra recorded by a nadir-looking instrument using the Earth's infrared emission as a source. Owing to pressure-broadening of the absorption lines, these instruments are mostly sensitive to tropospheric absorbers. The main absorption features in the 650-3000 cm^{-1} atmospheric spectral range are due to rotational transition lines related to the fundamental vibrational bands of H_2O, CO_2, O_3, N_2O, CH_4, and CO. To retrieve these species from the radiance spectra, channels with relevant information for inversion have to be selected. In an ideal situation, these spectral intervals would be located over the strongest absorption band of the molecule and should be sufficiently narrow to exclude the contaminating signal from other gases. Because of time and data rate constraints, use of selected narrow spectral intervals is also strongly recommended for routine retrieval.

Figure 4 and Figure 5 provide the simulated radiances at 0.1 cm^{-1} spectral resolution for mean atmospheric conditions (Air Force Geophysics Laboratory (AFGL) U.S. Standard Atmosphere 1976) in the spectral range where the main absorption bands of O_3, CH_4, and CO occur. In order to illustrate the contribution of foreign interfering gases which absorb in the same spectral range, the spectra were also calculated for the species alone. In the 980-1080 cm^{-1} spectral interval, most of the absorption features belong to the ν_3 vibrational band of O_3 (Figure 4a). Isolated H_2O lines and a weak CO_2 absorption band, between 1030 and 1080 cm^{-1}, explain the very small differences observed between the two subplots of Figure 4a. To retrieve methane from the atmospheric spectra, selected spectral ranges are to be chosen within either the 1200-1400 cm^{-1} or 2700-3000 cm^{-1} spectral interval, which contain the methane absorption lines associated with the ν_4 and ν_3 vibrational bands, respectively. Important interferences due to H_2O (which saturates the spectra above 1320 cm^{-1}) and N_2O (between 1240 and 1320 cm^{-1}) are responsible for the strong perturbations observed in the ν_4 band (Figure 4b), whereas the ν_3 band is mostly affected by water vapor lines (Figure 4c). Note that because of the IASI spectral range limitation at 2760 cm^{-1}, only a narrow part of the ν_3 band may be used for CH_4 retrieval from the IASI spectra. The top panel of Figure 5 represents the atmospheric spectra in the 2000-2250 cm^{-1}

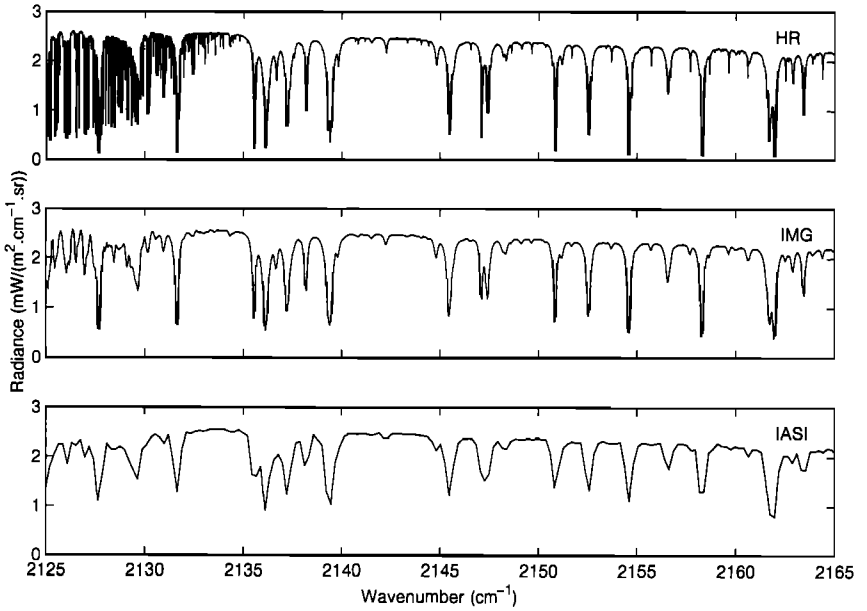

Figure 3. Radiance spectra for a nadir view in the 2125-2165 cm^{-1} spectral interval, simulated at a high spectral resolution (1 10^{-3} cm^{-1}), and for IMG and IASI instrumental characteristics.

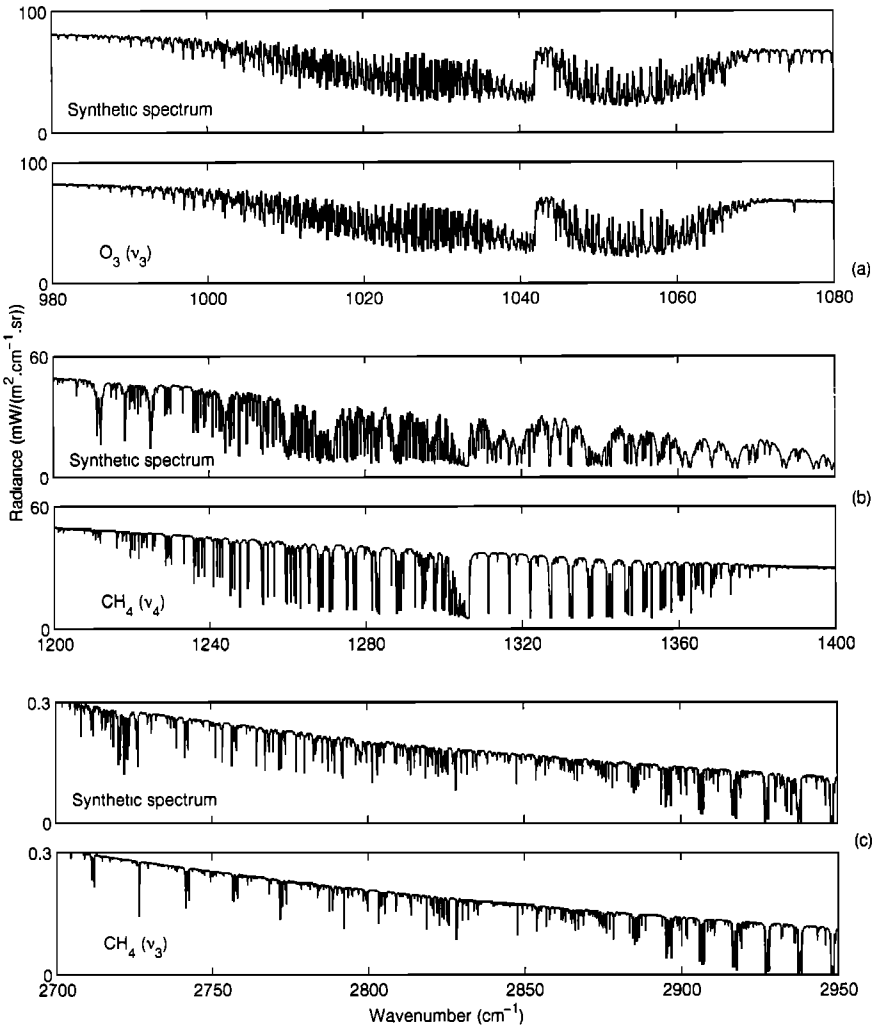

Figure 4. Simulated nadir radiance spectra at 0.1 cm^{-1} spectral resolution in the spectral range of (a) O_3 and (b) and (c) CH_4 retrieval, and corresponding main absorption bands for these molecules.

spectral range, where the intense 1-0 vibrational transition of CO occurs. In order to illustrate the difficulty of discriminating between the spectral signature of CO and other absorbing gases, the separated contribution of CO, H_2O, CO_2, O_3, and N_2O are also represented.

Within these main vibrational bands, a set of narrow spectral windows which minimize interferences has been selected in order to define the relevant intervals to be used in the inversion process for an efficient retrieval of O_3, CH_4, and CO. For each selected interval, the following criteria were applied: (1) intense and nonsaturated spectral signature of the target species (to increase signal to noise ratio) and (2) low contribution of interfering gases (preferably CO_2 or N_2O than H_2O or O_3, which have strong spatial variabilities). The AFGL Standard Atmosphere 1976 mixing ratio profiles were used for a first selection, and then a test set of IMAGES representative profiles allowed refinement of the proposed wavenumber limits. The latter are provided in Table 3, along with the spectroscopic identification of the main absorption features. Each selected interval contains either one single absorption line (CO, CH_4) or groups of unresolved lines merged into broad peaks (CH_4, O_3).

All the selections were carried out at high spectral resolution. When decreasing the spectral resolution, the wings of the instrumental function can introduce interferences from other gases with absorbing lines located outside the selected spectral range, but these intervals still remain less contaminated. A detailed study of this effect is given by *Chazette et al.* [1998]. According to their spectral resolution and sampling, IMG and IASI have different recording channels within these intervals. The corresponding available channels for each instrument are also provided in Table 3. By adding all the available channels for IMG and IASI, a total of 820 and 158 channels, respectively, are found for O_3, 884 and 36 for CH_4 (including both the ν_3 and the ν_4 bands), and 104 and 17 for CO.

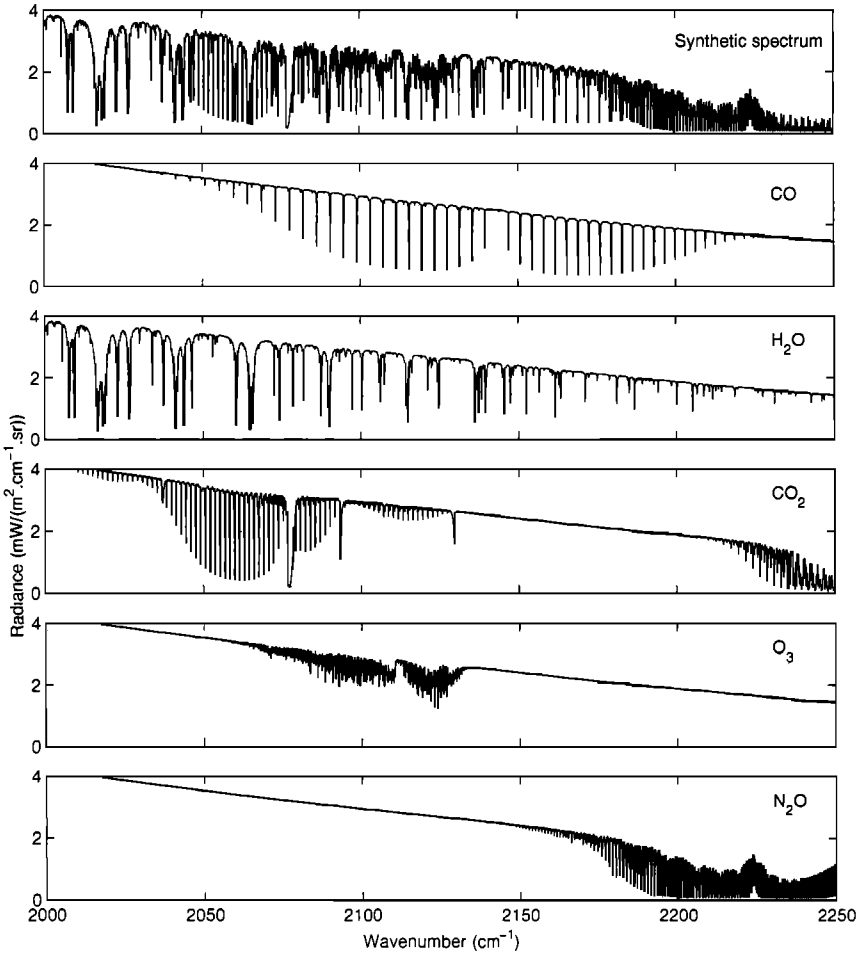

Figure 5. (top) Simulated nadir radiance spectra at 0.1 cm^{-1} spectral resolution in the spectral range of CO retrieval, and (remaining pannels) separated contribution for each absorbing gases (CO, H_2O, CO_2, O_3, and N_2O).

An efficient inversion algorithm for the retrieval of CO, CH_4, and O_3 should include several of these channels in order to improve the signal-to-noise ratio and to minimize the remaining weak contributions due to interfering gases (mainly H_2O). Calculation time sometimes limits the number of channels that can be introduced in the inversion scheme. Among all the intervals, those which best agreed with the high-intensity/ low-interference criteria are given in parentheses in Table 3. The sensitivity studies described hereinafter were performed using the four intervals footnoted in Table 3, which were found to be totally free from interfering constituents.

4. Sensitivity Studies

4.1. Measurement Accuracy

The radiances recorded by an infrared nadir-looking instrument are functions of trace gas concentrations, atmospheric temperature profile, surface emissivity, and instrumental characteristics (noise and resolution). Other parameters like clouds or aerosols may also affect the measurement. In this study, we assumed that all variables other than the gas concentration are known. The use of selected spectral intervals minimizes the uncertainty due to absorption of interfering gases. The surface emissivity over land is usually unknown, but use of differential radiance values (baseline substracted) reduces contributions from surface emissivity, aerosols, and, to a lesser extent, clouds. Most of the uncertainty on the measured radiances then comes from the instrumental noise and the use of a temperature profile that may be erroneous.

Both IMG and IASI missions have as measurement objectives the derivation of total column amounts for CO, CH_4, and O_3. A measurement accuracy <10% should be achieved for cloud and aerosol-free conditions [*Diebel et al.*, 1996]. Retrieval of low-resolution vertical profiles will also be undertaken for these species. This section attempts to discuss these requirements and compare them with the expected variability of each species.

To perform these sensitivity studies, we used the large data set of radiances associated with realistic mixing ratio profiles for CO, O_3, and CH_4 that was created

Table 3. Selected Spectral Intervals for O_3, CH_4, and CO, Identification of the Main Absorption Features, and Corresponding Number of Channel Available for IMG and IASI

Retrieved Molecule	Spectral Interval, cm^{-1}	Identification	IMG Channels	IASI Channels
O_3	(1001.3-1003.4)	ν_3 P lines	42	8
O_3	1004.6-1009.7	ν_3 P lines	102	20
O_3	1011.7-1014.1	ν_3 P lines	47	9
O_3	(1014.9-1017.2)	ν_3 P lines	45	9
O_3	(1018.4-1027.6)[a]	ν_3 P lines	183	36
O_3	1033.7-1035.3	ν_3 P,Q lines	32	6
O_3	(1035.7-1037.3)	ν_3 P,Q lines	32	6
O_3	1038.3-1039.2	ν_3 P,Q lines	17	3
O_3	1039.8-1041.1	ν_3 P,Q lines	25	5
O_3	1041.5-1042.4	ν_3 Q lines	18	3
O_3	(1043.3-1044.8)	ν_3 R lines	30	6
O_3	1045.2-1046.7	ν_3 R lines	30	6
O_3	1047.0-1048.2	ν_3 R lines	23	4
O_3	1049.6-1050.1	ν_3 R lines	10	2
O_3	1052.4-1053.7	ν_3 R lines	25	5
O_3	1054.1-1055.3	ν_3 R lines	24	4
O_3	1055.8-1057.1	ν_3 R lines	25	5
O_3	1057.5-1058.4	ν_3 R lines	18	3
O_3	(1059.1-1059.9)	ν_3 R lines	16	3
O_3	1060.7-1062.0	ν_3 R lines	26	5
O_3	1063.0-1065.5	ν_3 R lines	50	10
CH_4	1219.5-1219.8	ν_4 P(12)	6	1
CH_4	(1228.6-1229.0)	ν_4 P(11)	8	1
CH_4	1229.8-1230.5	ν_4 P lines	13	2
CH_4	1235.7-1236.1	ν_4 P lines	8	1
CH_4	(1237.9-1238.8)[a]	ν_4 P lines	18	3
CH_4	(1240.7-1242.1)	ν_4 P lines	28	5
CH_4	1245.5-1246.6	ν_4 P lines	21	4
CH_4	(1249.8-1250.2)	ν_4 P(9)	7	1
CH_4	1253.7-1253.9	ν_4 P lines	4	0
CH_4	1254.9-1255.2	ν_4 P(8)	5	1
CH_4	1256.5-1256.8	ν_4 P(8)	6	1
CH_4	1263.1-1263.5	ν_4 P(7)	8	1
CH_4	1274.8-1275.3	ν_4 P(5)	10	2
CH_4	1277.4-1277.6	ν_4 P(5)	3	0
CH_4	1282.5-1282.9	ν_4 P(4)	8	1
CH_4	1292.5-1292.7	ν_4 P,Q lines	3	0
CH_4	1294.2-1294.5	ν_4 P(1)	6	1
CH_4	1316.5-1317.0	ν_4 R(1)	10	2
CO	2086.1-2086.5	1-0 P(14)	7	1
CO	(2111.3-2111.7)	1-0 P(8)	7	1
CO	2123.4-2124.0	1-0 P(5)	12	2
CO	(2127.4-2128.0)	1-0 P(4)	12	2
CO	2131.3-2131.9	1-0 P(3)	11	2
CO	2150.7-2151.1	1-0 R(1)	8	1
CO	(2158.0-2158.6)[a]	1-0 R(3)	12	2
CO	(2165.4-2165.9)	1-0 R(5)	10	2
CO	(2169.0-2169.5)	1-0 R(6)	10	2
CO	2172.5-2172.9	1-0 R(7)	7	1
CO	2176.2-2176.6	1-0 R(8)	8	1
CH_4	2726.5-2726.8	ν_3 P lines	6	1
CH_4	(2741.0-2743.0)[a]	ν_3 P lines	40	8
CH_4	2771.5-2771.8	ν_3 P(4)	6	...
CH_4	2773.3-2774.0	ν_3 P(4)	13	...
CH_4	2792.1-2792.4	ν_3 P(3)	5	...
CH_4	2818.4-2818.8	ν_3 Q(3)	8	...
CH_4	2825.1-2826.0	ν_3 Q lines	17	...
CH_4	(2847.5-2847.9)	ν_3 R(0)	7	...
CH_4	2873.5-2878.5	ν_3 R lines	100	...
CH_4	2883.0-2889.0	ν_3 R lines	120	...
CH_4	(2894.5-2901.0)	ν_3 R lines	130	...
CH_4	2905.4-2906.0	ν_3 R lines	12	...

Table 3. (continued)

Retrieved Molecule	Spectral Interval, cm^{-1}	Identification	IMG Channels	IASI Channels
CH_4	2910.4-2910.8	ν_3 R(6)	8	...
CH_4	(2915.5-2918.0)	ν_3 R lines	50	...
CH_4	(2926.0-2928.5)	ν_3 R lines	50	...
CH_4	2947.0-2950.0	ν_3 R lines	60	...
CH_4	2957.5-2959.5	ν_3 R lines	40	...
CH_4	2998.0-3000.0	ν_3 R lines	40	...

Intervals in parentheses are those that best agreed with the high-intensity/low-interference criteria.

[a] The sensitivity studies were performed using this interval.

by introducing the 2520 vertical profiles provided per month by the 3-D IMAGES model into the LBLRTM radiative code.

4.2. Instrumental Noise

In order to simulate the contribution of the instrumental noise to the signal, each radiance spectra was also randomly perturbed using the noise characteristics provided in Figure 1. Averaged uncertainties on radiances due to instrumental noise were found to be lower than 1% for O_3 and $CH_4(\nu_4)$, 6% for CO, and 10% for $CH_4(\nu_3)$.

4.3. Vertical Temperature Profile

Temperature profiles are usually measured by observing the upwelling spectral radiance of the main vibrational bands of CO_2. Thanks to the high spectral resolution of the forthcoming instruments, it is expected that temperature could be retrieved with accuracies of 1 K (RMS) at vertical resolution of 1 km, at least in the lower troposphere [*Diebel et al.*, 1996]. In this section, we study how the use of an erroneous temperature profile impacts the calculated radiances and hence the retrieval accuracy.

To perform realistic simulations, we made use of an error covariance matrix provided by Meteo-France which is represented in Figure 6. This matrix characterizes the accuracy associated with the retrieval of a temperature profile on 21 levels, using the IASI instrumental characteristics. It was assumed that temperature determination could be achieved with at least a similar accuracy when analyzing the IMG spectra. A test set of standard temperature profiles has been defined and then randomly perturbed using this error covariance matrix. We estimated the impact of the use of an erroneous profile by calculating the differences between the radiances obtained using the reference temperature profiles and using a set of corresponding noisy profiles, in each spectral interval and at each instrumental resolution. In all cases, the use of an erroneous temperature profile leads to a relative error on the calculated radiance that does not exceed 0.5%, which is thus always below the noise level. As an example, a polar temperature profile with two profiles perturbed with random noise, their associated radiances in the CO 2157.8-2158.6 cm^{-1} spectral range, and the relative differences compared to the noise level are plotted in Figure 6.

As the spectra obtained by nadir-looking instruments use the thermal emission of Earth as a source, the temperature dependence of each calculated radiance is determined by both the temperature dependence of its absorption coefficients and of the Planck function. Owing to the shape of the latter, the impact of an error on the temperature profile increases as a function of wavenumbers. As expected, the species absorbing at lower wavenumbers (O_3, CH_4-ν_4) are even less affected than those absorbing at higher wavenumbers (CO, CH_4-ν_3).

4.4. Spatial and Temporal Variability

From the monthly-mean tropospheric mixing ratio profiles simulated by the IMAGES model, we calculated total column amounts for CO, CH_4, and O_3, each $5^o \times 5^o$, for each month. Large variabilities are observed above continents, as a function of latitude, longitude, and season. The amplitude of the change in total column is directly related to the average lifetime of the species, which is estimated to about 2 months and 10 years for CO and CH_4, respectively, and ranges from a few weeks (low troposphere) to 3 months (high troposphere) for O_3 [*Müller and Brasseur*, 1995]. Because of its long lifetime the distribution of methane in the troposphere is nearly homogeneous, and its seasonal change is small.

The global variability of each constituent at the spatial and temporal resolution of the IMAGES model may be quantified by analyzing the change in its total column value at a fixed time period (month fixed) or by observing the change in concentration at a given location (longitude and latitude fixed) during the 12 months of the simulation. The results are summarized in Table 4, which presents for each constituent the relative difference (in percent) between the minimum and the maximum values, as well as the standard deviation (1σ in percent) for both spatial and temporal variabil-

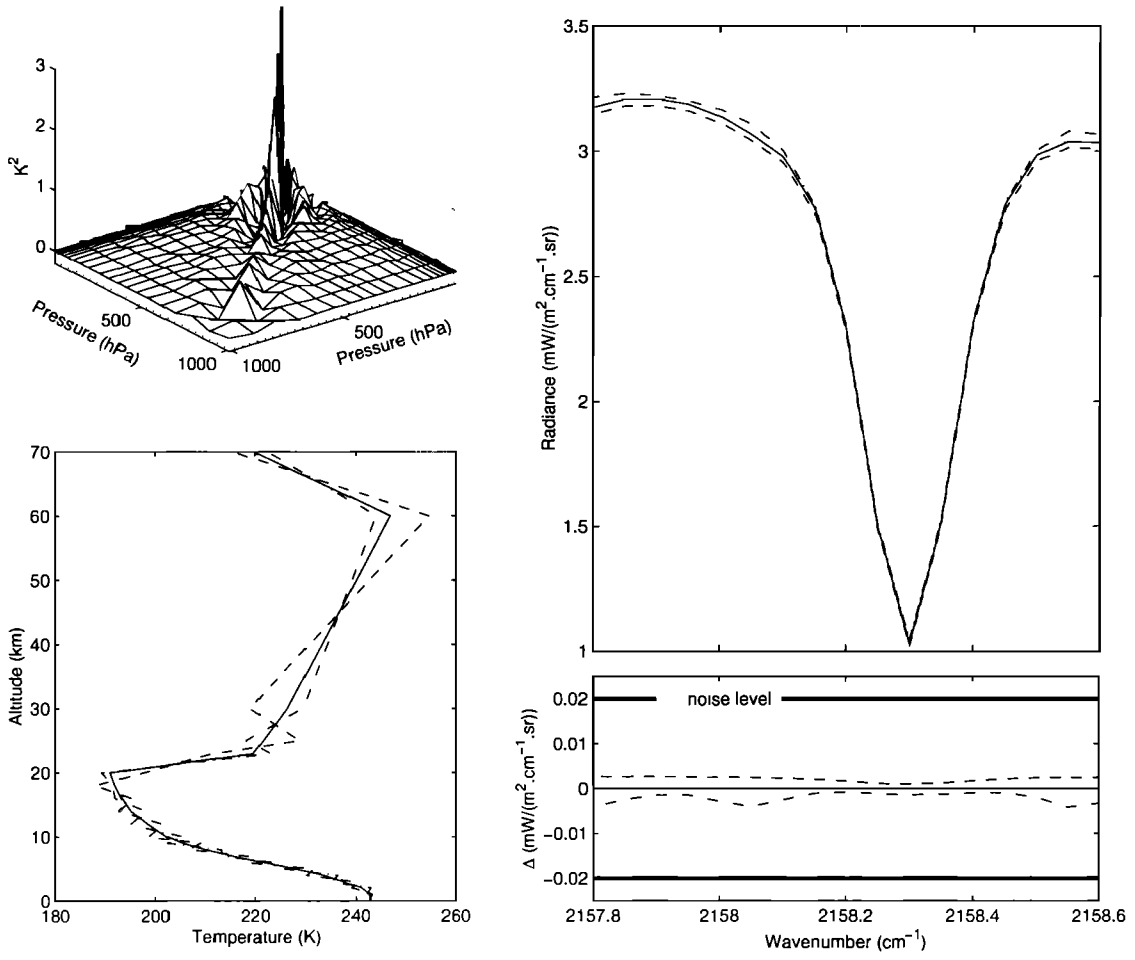

Figure 6. (left) Temperature error covariance matrix (top) and temperature profiles used for the simulation (bottom). The initial temperature profile is represented by a solid line, whereas the two noisy profiles calculated using the error covariance matrix are represented in dashed lines. (right) Associated calculated radiances (0.1 cm^{-1} spectral resolution) in the 2157.8-2158.6 cm^{-1} spectral range and differences between the three radiance spectra. The level of noise (2 10^{-2}mW/(m^2 cm^{-1} sr)) is also indicated for comparison.

ities. These values should be considered as approximative due to the use of the IMAGES database. Indeed, the limitations of the model (monthly-means and limited at 50 mbar) lead to calculated variabilities that may be underestimated compared with the real atmospheric variabilities. In particular, the IMAGES model does not represent correctly the ozone variability at the tropopause (troposphere/stratosphere exchanges). A detailed comparison between the model results and the available observations, which are generally in good agreement, is given by *Müller and Brasseur* [1995].

From these values, it can be observed that if the 10% accuracy requirement is achieved, measurements of changes in CO and O_3 total columns, which both have temporal and spatial variabilities exceeding this value, would be allowed. It is not the case for methane,

Table 4. Changes in Total Columns on Spatial and Temporal Scales for the IMAGES Database (Below 50 mbar)

Variability	CO		CH_4		O_3	
	Spatial	Temporal	Spatial	Temporal	Spatial	Temporal
Maximum/minimum	300	90	10	5	800	200
Standard deviation (1σ)	33.5	22.5	2.5	1.5	49	43

All values ares given in percent.

for which a maximum change of 10% in total content was found. A better accuracy than 10% would then be needed in order to provide useful measurements for this species.

4.5. Vertical Mixing Ratio Profile

To create the database, a fixed mean temperature profile was used for each run, in order to assess the sensitivity of the calculated radiances (in the spectral intervals defined above) to the vertical distribution of the species studied. As expected, we found that radiances are strongly correlated to total column amounts. We observed, however, that some mixing ratio profiles, corresponding to different total column amounts, can provide similar atmospheric spectra when taking noise into account. As an example, Figure 7 shows three selected IMAGES CO mixing ratio profiles, which correspond to total column amounts of 1.78×10^{18}, 1.95×10^{18}, and 2.24×10^{18} molecules/cm^2. The associated calculated radiance spectra in the 2157.8-2158.6 cm^{-1} interval, also plotted in Figure 7, are found to be very close, as may be checked by considering the differences between these three radiance spectra which are represented along with the level of noise. When taking noise into account, it can be seen that a similar signal is obtained for these three profiles and that the information on the shape of the profile is lost. This remains true when using the other selected intervals for CO. It means that the sensitivity of the measured radiances on the change of CO profile in the boundary layer is weak.

We tried to generalize this observation to the entire data set. We identified the profiles that provide the same spectra if noise is taken into account. We then calculated the mean value and the standard deviation of the corresponding total column amounts. Figure 8 represents the coefficient of variation (standard deviation/mean value) from a mean total column value, for CO and O_3. The most important values are observed for CO, which combines at the same time a high variability and a high instrumental noise contribution. It can be observed that the dispersion increases with concentration. High values were found for high concentrations, mainly due to the low number of IMAGES data available, as can be observed on the histogram also represented in Figure 8. For this molecule, half of the 2520 IMAGES profiles have a relative dispersion lower than

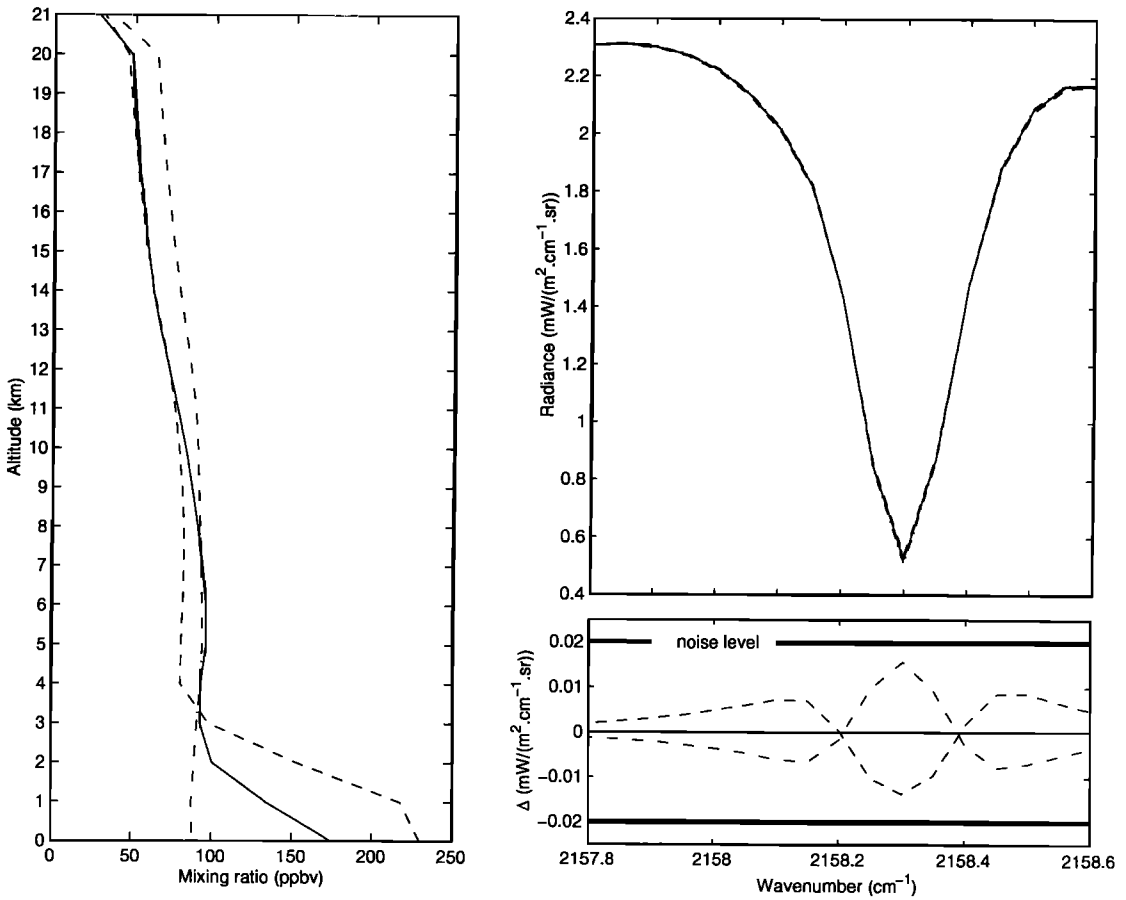

Figure 7. (left) Selected CO mixing ratio profiles. (right) Associated calculated radiances (0.1 cm^{-1} spectral resolution) in the 2157.8-2158.6 cm^{-1} spectral range and differences between the three radiance spectra. The level of noise (2 10^{-2} mW/(m^2 cm^{-1} sr)) is also indicated for comparison.

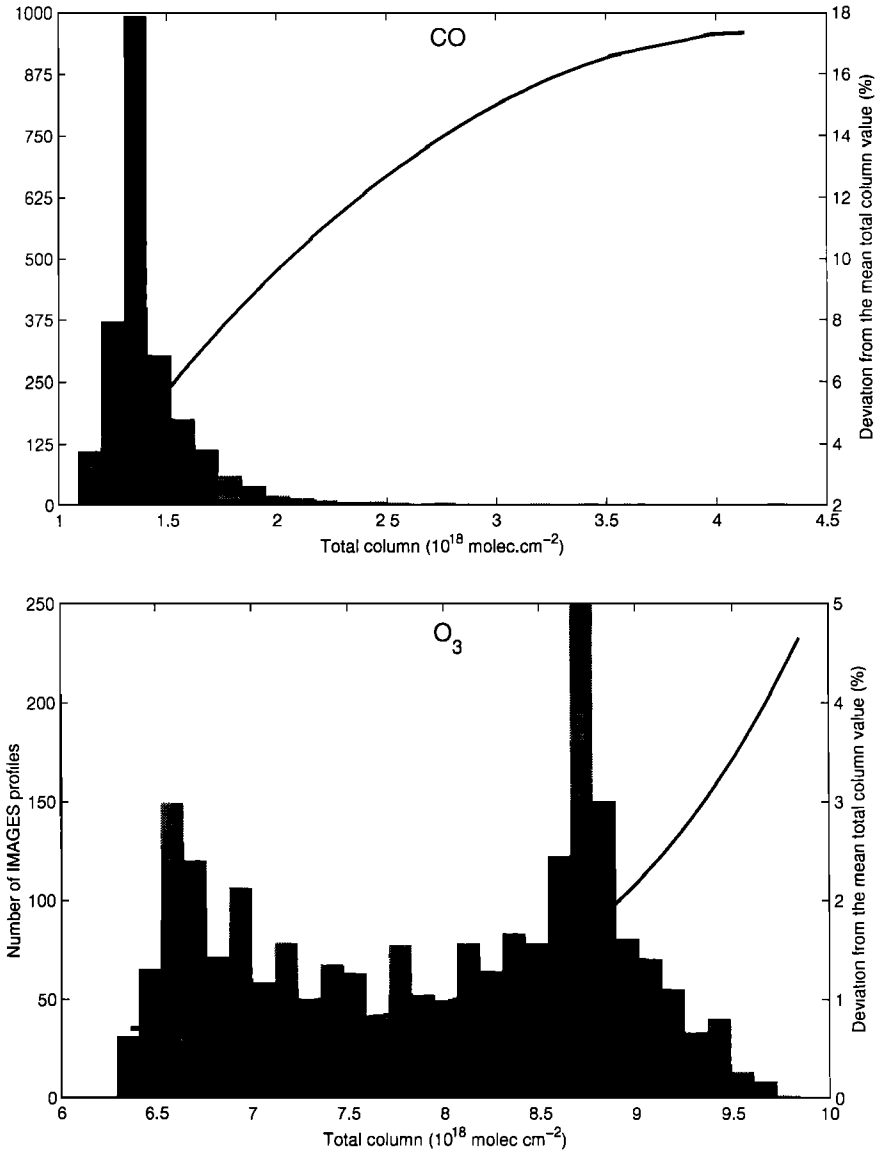

Figure 8. Standard deviation (in percent) from a mean total column value for CO and O_3 IMAGES profiles which provide similar spectra when noise is included in the simulation, as a function of the mean total column. An histogram of the dispersion of the total columns calculated from the IMAGES profiles (month of July) is also provided.

5%, and 1% of the data exceeds the required 10% limit of retrieval accuracy. A similar work has been undertaken on O_3, which also has a high variability but a much lower noise contribution. The results are also represented in Figure 8, and it can be observed that in this case, due to the low noise level and high number of radiance channels, the change in vertical profiles leads to errors not exceeding 2% for 90% of the database. Finally, due to its low geographic variability, this effect is negligible for methane.

Being a tropospheric model, the IMAGES model provides mixing ratio profiles limited to 50 hPa (~21 km). In order to assess the contribution of the upper part of the profile on the calculated nadir radiances, simulations were performed using a fixed tropospheric profile and the 6 AFGL standard atmospheres for altitudes above 21 km. For all radiance channels belonging to the selected intervals (see Table 3), we have calculated the relative differences between the radiances associated with the U.S. 1976 Standard Atmosphere profile and the five other standard profiles. As expected, the most important variations were found for all three compounds for radiances located at the center of the line, or absorption feature, which are more sensitive to the higher levels of the atmosphere. These values remain very low, however, reaching 1.2% for ozone, which exhibits a strong increase in mixing ratio above 20 km, 0.7% for CO, which strongly increases above 60 km due to photodissociation of CO_2, and 0.07% for CH_4. By comparing these values to uncertainties on radiances

due to noise (1% for O_3, 6% for CO and CH_4), it can be seen that, by using a nadir-viewing instrument, the information on trace gas content for altitudes exceeding 20 km is lost into the instrumental noise. At these altitude levels, only ozone induces a detectable contribution on the measured spectra.

5. Climatological Profiles

Most of the retrieval algorithms rely on a first-guess profile for initialization of the inversion process. Also, for the retrieval of water vapor and temperature, representative profiles of trace gases are generally required. Standard model atmospheres, as the commonly used AFGL profiles for mean tropical, midlatitude, and polar atmospheres, are often used as a source of profiles to generate spectra representative of a typical air mass. There are two major limitations when using such model atmospheres. First, trace gases with strong emission sources have distributions with large temporal and spatial variabilities, which generally do not match with a latitudinal air mass representation. Second, these standard atmospheres do not encompass the full range of extremes encountered in a real atmosphere in terms of constituent concentration.

In order to provide mean profiles representative of the spatiotemporal variability of each species, a statistical classification has been performed on the IMAGES database to build a reduced climatological database. In the section 4, we concluded that some concentration profiles could provide similar spectra. For each month and each constituent, a standard statistical method of classification has been applied to the calculated radiances data set to gather vertical mixing ratio profiles associated with close radiance spectra in the same class. We used a classical agglomerative hierarchical clustering method [*Anderson*, 1958], which maximizes the variance between the classes using the calculated radiances as classification parameter. The agglomerative clustering procedure is stopped when the variance associated with the classification reaches 90%. A mean concentration profile is then calculated by averaging all the atmospheric profiles of each class. We checked that profiles which belong to two separated classes have associated spectra that could at least be distinguished when taking noise into account.

The climatological values profiles derived from the classification of CO for the month of July are plotted in Figure 9. These profiles are representative of the main distribution of CO, as can be observed in Figure 10, which provides (top) the CO total columns calculated from the outputs of IMAGES and (bottom) the result of the classification. Figure 10 clearly shows that because of its short lifetime and seasonally varying sources and sink, the distribution of CO could not be represented in terms of latitude dependent air masses. A similar work has been performed for each month and for the three species. For CO and O_3, strong latitudinal variabilities are found with amplitudes varying as a function of time. For CH_4, due to its longer lifetime and thus lower variability, the geographical distribution of the standard profiles is close to a latitude dependent air mass classification, except above high emission sources.

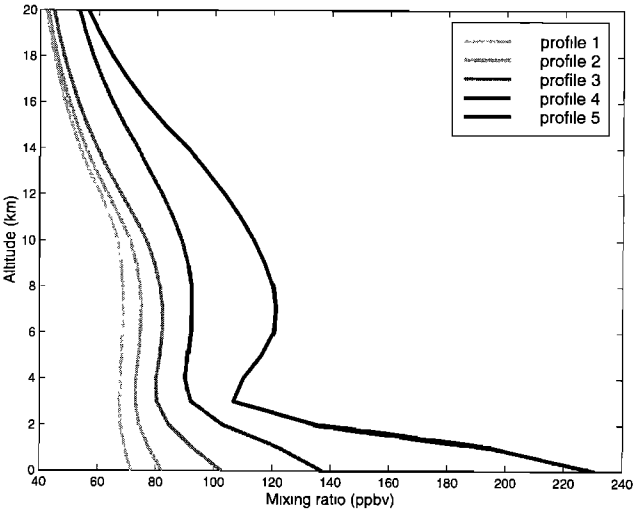

Figure 9. Climatological vertical profiles for CO in July.

We also used our extended profile database to select a minimum concentration profile (corresponding to a geographical point where there is no source) and a maximum concentration profile (intense sources) for each species. The profiles associated with the lower and higher concentrations in terms of total column amounts were chosen. Files with minimum, maximum, and standard concentration profiles (along with their geographical distribution) are available upon request through anonymous ftp.

6. Conclusions and Discussion

Most of the inversion algorithms presently under development for the retrieval of trace gases from nadir radiances spectra are designed to use selected spectral intervals and also need a priori profiles for initialization. In order to meet these requirements, we provide a range of spectral windows for an efficient retrieval of total column amounts for CO, CH_4, and O_3 as well as a set of representative climatological profiles.

The simultaneous retrieval of these three compounds on a global scale from spectra provided by nadir-viewing instruments will enhance our knowledge and understanding of the troposphere. Due to their different natural variabilities and spectroscopic properties, however, the retrievable information is very different for CO, CH_4, and O_3. The sensitivity studies undertaken here are aimed at studying these differences for an infrared nadir-viewing Fourier transform interferometer and providing quantified values using IMG and IASI instrumental noise and resolution characteristics.

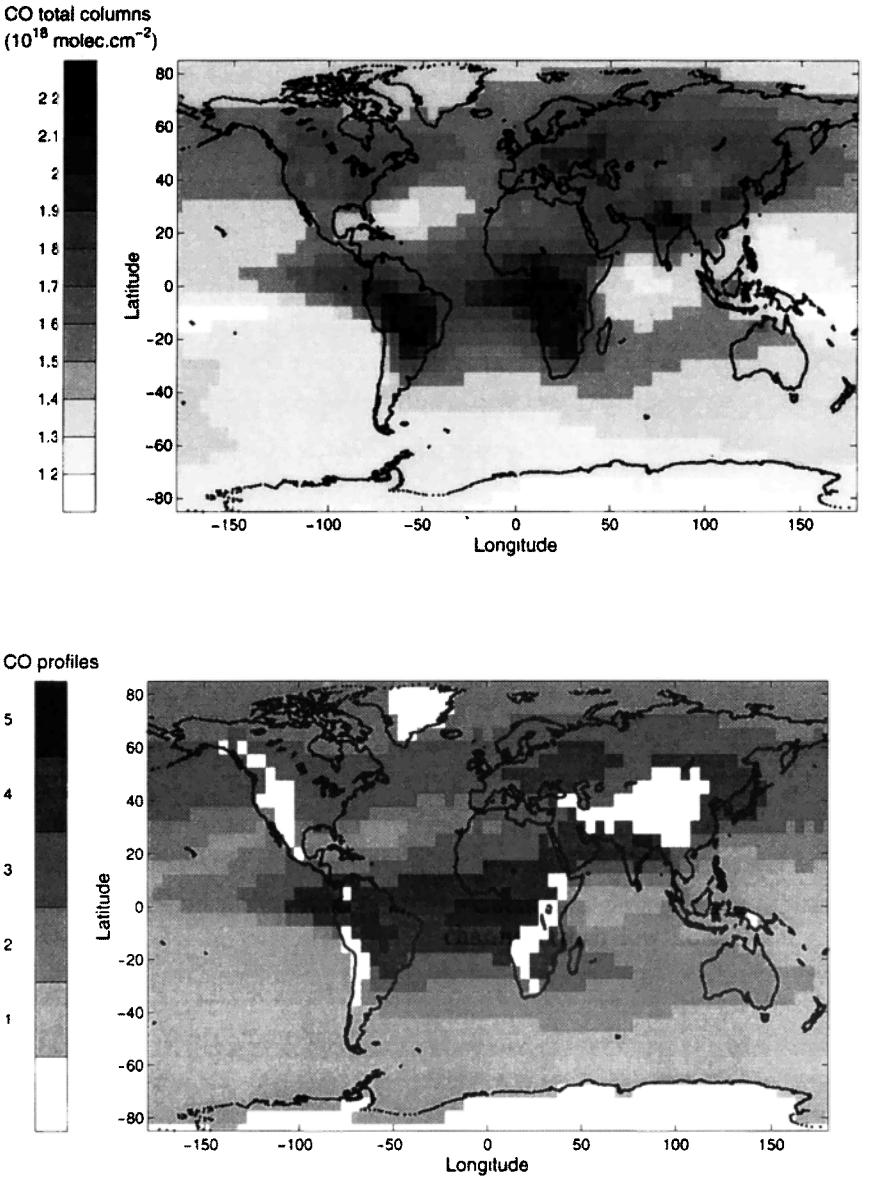

Figure 10. (top) CO total columns as provided by the IMAGES model for July and (bottom) geographic distribution of the climatological profiles. The label and color associated to each profile are those of Figure 9. Profiles corresponding to sea levels exceeding 1 km were not included in the classification and are shown in white.

6.1. Carbon Monoxide

This study shows that despite its large natural variability, the retrievable information is limited for CO due to its narrow IR spectral signature with a relatively high associated signal-to-noise ratio. As several interfering molecules absorb in the same spectral range, there is only a very limited number of useful channels for inversion. For the largest concentrations, where the 10% requirement for inversion accuracy may not be fulfilled, spatial average of successive measurements would increase the signal-to-noise ratio. The retrievable information is restricted to altitudes below 20 km. The use of standard atmospheres based on latitude air masses is not recommended for CO.

6.2. Methane

The accuracy to be achieved by inversion procedures should be lower than the 10% requirement in order to be able to detect some changes in the methane concentration using this kind of instrument. Although the available channels of the ν_3 band are less affected by perturbations due to interfering species than those of the ν_4 band, the large contribution of noise at this spectral range makes the latter more useful. Standard atmospheres based on latitude air masses may be used as first-guess profiles.

6.3. Ozone

Ozone has a large natural variability. A lot of clean channels with low noise level associated are available

for inversion. Total column amounts could be retrieved with good accuracy. The stratospheric part of the profile also contributes to the radiance spectra. Use of standard atmospheres based on latitude air masses is not recommended.

6.4. Discussion

The retrieval of vertical concentration profiles instead of total column amounts is a difficult task due to the nadir-viewing mode of the IMG and IASI-like instruments, which scan all the atmospheric layers at the same time. With the combined use of several radiance channels with associated weighting functions peaking at different levels of altitude, some information on the vertical profiles may be retrieved with an accuracy highly dependent on the instrumental spectral resolution. That study is beyond the scope of the present paper, but a rapid assessment of the useful radiance channels available for the retrieval of each species (see section 3) shows that the information is very limited for CO and CH_4, particularly at IASI spectral resolution. For O_3, the retrieval of some layers in the troposphere and also one stratospheric layer should be possible.

If these nadir-looking instruments succeed in retrieving temperatures with a 1-K RMS accuracy in the troposphere, then our simulations showed that the impact on recorded radiances is below the instrumental noise level.

Finally, in this simulation, neither uncertainties due to the direct model (e.g., precision on the spectroscopic parameters, knowledge of the molecular continua) nor the efficiency of the inversion procedure were taken into account. The values provided here should be considered as minimum error limits which could be expected when using nadir spectral radiances in retrieval algorithms. We will check these results with real data as soon as the IMG data become available.

Acknowledgments. We are grateful to Claude Camy-Peyret for helpful discussions and for providing the IASI ISRF. Pascal Prunet (Meteo-France) is acknowledged for providing the IASI temperature error covariance matrix. This work was undertaken in the framework of the ISSWG (IASI Sounding Science Working Group) activities under the auspices of EUMETSAT (European Organisation for the Exploitation of Meteorological Satellites) and CNES (Centre National d'Etudes Spatiales). J.-F. Müller is supported by a grant from the Belgian Office for Scientific, Technical and Cultural Affairs (OSTC).

References

Anderson, T. W., *An Introduction to Multivariate Statistical Analysis*, John Wiley, New York, 1958.

Aumann, H. H., and C. Miller, Atmospheric infrared sounder (AIRS) on the Earth Observing System: Advanced and next-generation satellites, *Proc. SPIE, Int. Soc. Opt. Eng.*, *2583*, 332-338, 1995.

Beer, R., and T. A. Glavich, Remote sensing of the troposphere by infrared emission spectroscopy, *Proc. SPIE, Int. Soc. Opt. Eng.*, *1129*, 42-48, 1989.

Brown, M., The singular value decomposition method applied to the deduction of the emissions and the isotopic composition of atmospheric methane, *J. Geophys. Res.*, *100*, 11,425-11,446, 1995.

Camy-Peyret, C., and S. Payan, A parametric representation of the instrumental response function of IASI: A contribution of LPMA to the ISSWG activities, internal report CNES/EUMETSAT, Paris, 1997.

Cayla, F., and P. Javelle, IASI instrument overview: Advanced and next-generation satellites, *Proc. SPIE, Int. Soc. Opt. Eng.*, *2583*, 271-281, 1995.

Chazette, P., C. Clerbaux, and G. Mégie, Direct estimate of the methane radiative forcing using nadir spectral radiances, Appl. Opt., *37*(15), 3113-3120, 1998.

Cheruy, F., N. A. Scott, R. Armante, B. Tournier, and A. Chedin, Contribution to the development of radiative transfer models for high spectral resolution observation in the infrared, *J. Quant. Spectrosc. Radiat. Transfer*, *53*(6), 597-611, 1995.

Clerbaux, C., P. Chazette and G. Mégie, Tropospheric concentrations of infrared absorbing molecules using a nadir-looking Fourier transform spectrometer: Passive infrared remote sensing of clouds and the atmosphere III, *Proc. SPIE, Int. Soc. Opt. Eng.*, *2578*, 148-153, 1995.

Clough, S. A., and M. J. Iacono, Line-by-line calculation of atmospheric fluxes and cooling rates, 2, Application to carbon dioxide, ozone, methane, nitrous oxide, and the halocarbons, *J. Geophys. Res.*, *100*, 16,519-16,535, 1995.

Clough, S. A., M. J. Iacono, and J.-L. Moncet, Line-by-line calculation of atmospheric fluxes and cooling rates, 1, Application to water vapor, *J. Geophys. Res.*, *97*, 15,761-15,785, 1992.

Clough, S. A., C. P. Rinsland, P. D. Brown, Retrieval of tropospheric ozone from simulations of nadir spectral radiances as observed from space, *J. Geophys. Res.*, *100*, 16,579-16,593, 1995.

Crutzen, P. J., A discussion of the chemistry of some minor constituents in the stratosphere and troposphere, *Pure Appl. Geophys.*, *106-108*, 1385-1399, 1973.

Diebel, D., F. Cayla, T. Phulpin, P. Courtier, and M. Langevin, IASI: Mission rationale and requirements, *IA-SM-0000-10-CNE/EUM*, pp. 1-36, CNES/EUMETSAT, Darmstadt, 1996.

Dlugokencky, E. J., L. P. Steele, P. M. Lang, and K. A. Masarie, The growth rate and distribution of atmospheric methane, *J. Geophys. Res.*, *99*, 17,021-17,043, 1994.

Dlugokencky, E. J., E. G. Dutton, P. C. Novelli, P. P. Tans, K. A. Masarie, K. O. Lantz, and S. Modronich, Changes in CH_4 and CO growth rates after the eruption of Mount Pinatubo and their link with changes in tropical tropospheric UV flux, *Geophys. Res. Lett.*, *23*, 2761-2764, 1996.

Drummond, J. R., and G. S. Mand, The measurement of pollution in the troposphere (MOPITT) instrument: Overall performances and calibration requirements, *J. Atmos. Oceanic. Technol.*, *13*, 314-320, 1996.

Fisher, M. and D. J. Lary, Lagrangian 4-Dimensional variational data assimilation of Chemical-species, *Q. J. R. Meteorol. Soc.*, *121*(527A), 1681-1704, 1995.

Granier, C., J. F. Müller, S. Madronich, and G. P. Brasseur, Possible causes for the 1990-1993 decrease in the global tropospheric CO abundances: A 3-dimensional sensitivity study, *Atmos. Environ.*, *30*(10/11), 1673-1682, 1996.

Intergovernmental Panel on Climate Change (IPCC), Climate Change 1995: *The Science of Climate Change*, edited by J. T. Houghton et al. Cambridge Univ. Press, New York, 1996.

Logan, J. A., M. J. Prather, S. C. Wofsy, and M. B. McElroy, Tropospheric chemistry: A global perspective, *J. Geophys. Res* *86*. 7210-7254, 1981.

McMillan, W. W., L. L. Strow, B. G. Doddridge, W. L. Revercomb, and H. L. Huang, Retrieval of carbon monoxide column densities using AIRS on EOS: Validation of a prototype retrieval algorithm, *Proc. SPIE, Int. Soc. Opt. Eng.*, *2830*, 169-179, 1996.

Müller, J.-F., and G. Brasseur, IMAGES: A three-dimensional chemical transport model of the global troposphere, *J. Geophys. Res.*, *100*, 16,445-16,490, 1995.

Novelli, P. C., L. P. Steel, and P. P. Tans, Mixing ratios of carbon monoxide in the troposphere, *J. Geophys. Res.*, *97*, 20,731–20,750, 1992.

Novelli, P. C., K. A. Masarie, P. P. Tans, and P. M. Lang, Recent changes in atmospheric carbon monoxide, *Science*, *263*, 1587-1590, 1994.

Ogawa, T., H. Shimoda, M. Hayashi, R. Imasu, A. Ono, S. Nishinomiya, and H. Kobayashi, IMG: Interferometric measurement of greenhouse gases from space, *Adv. Space. Res.*, *14*, 25-28, 1994.

Pan, L., D. P. Edwards, J. C. Gille, M. W. Smith, and J. R. Drummond, Satellite remote sensing of tropospheric CO and CH_4: Forward model studies of the MOPITT instrument, *Appl. Opt.*, *34* (30), 6976-6988, 1995.

Rothman, L. S., et al., The HITRAN molecular database: Editions of 1991 and 1992, *J. Quant. Spectrosc. Radiat. Transfer*, *48*(5/6), 469-507, 1992.

Wetzel, G., H. Fisher, and H. Oelhaf, Remote sensing of trace gases in the midinfrared spectral region from a nadir view, *Appl. Opt.*, *34*(3), 467-479, 1995.

World Meteorological Organization (WMO), Scientific assessment of ozone depletion: 1994, Global Ozone Research and Monitoring Project, *Rep. 37*, Geneva, 1995.

P. Chazette, Laboratoire des Sciences, du Climat et de l'Environnement, CEA, L'Ormes des Merisiers, Saclay, France. (e-mail: pch@asterix.saclay.cea.fr)

C. Clerbaux, J. Hadji-Lazaro, and G. Mégie, Service d'Aéronomie du CNRS, Université Paris 6, BP 102, 75252 Paris Cedex 05, France. (e-mail: cathy.clerbaux@aero.jussieu.fr)

S. A. Clough, Atmospheric & Environmental Research, Inc., 840 Memorial Drive, Cambridge, MA 02139. (e-mail: clough@aer.com)

J.-F. Müller, Belgian Institute for Space Aeronomy, 3, av. Circulaire, 1180 Bruxelles, Belgium. (e-mail:jean-francois.muller@bira-iasb.oma.be)

(Received January 27, 1998; revised April 16, 1998; accepted April 22, 1998.)